Development and evaluation of injectable nanosized drug delivery systems for apigenin

Reatul, Karim; Palazzo, Claudio; Laloy, Julie; Delvigne, Anne-Sophie; Vanslambrouck, Stéphanie; Jérôme, Christine; Lepeltier, Elise; Orange, Francois; Dogné, Jean-Michel; Evrard, Brigitte; Passirani, Catherine; Piel, Géraldine

Published in:
International Journal of Pharmaceutics

DOI:
10.1016/j.ijpharm.2017.04.064

Publication date:
2017

Document Version
Publisher's PDF, also known as Version of record

International Journal of Pharmaceutics 532 (2017) 757–768

Contents lists available at ScienceDirect

International Journal of Pharmaceutics

journal homepage: www.elsevier.com/locate/ijpharm

Development and evaluation of injectable nanosized drug delivery systems for apigenin

Reatul Karim[a,d,*], Claudio Palazzo[a], Julie Laloy[b], Anne-Sophie Delvigne[b], Stéphanie Vanslambrouck[c], Christine Jerome[c], Elise Lepeltier[d], Francois Orange[e], Jean-Michel Dogne[b], Brigitte Evrard[a], Catherine Passirani[d], Géraldine Piel[a]

[a] Laboratory of Pharmaceutical Technology and Biopharmacy, CIRM, University of Liege, Liege, Belgium
[b] Namur Nanosafety Centre, NARILIS, Department of Pharmacy, University of Namur, Namur, Belgium
[c] Center for Education and Research on Macromolecules (CERM), University of Liege, UR-CESAM, Liege, Belgium
[d] MINT, UNIV Angers, INSERM 1066, CNRS 6021, Université Bretagne Loire, Angers, France
[e] Université Côte d'Azur, Centre Commun de Microscopie Appliquée, Nice, France

ARTICLE INFO

Article history:
Received 3 February 2017
Received in revised form 21 April 2017
Accepted 25 April 2017
Available online 27 April 2017

Keywords:
Apigenin
Liposome
Lipid nanocapsule
Polymeric nanocapsule
Injectable nanocarrier

ABSTRACT

The purpose of this study was to develop different injectable nanosized drug delivery systems (NDDSs) i.e. liposome, lipid nanocapsule (LNC) and polymeric nanocapsule (PNC) encapsulating apigenin (AG) and compare their characteristics to identify the nanovector(s) that can deliver the largest quantity of AG while being biocompatible. Two liposomes with different surface characteristics (cationic and anionic), a LNC and a PNC were prepared. A novel tocopherol modified poly(ethylene glycol)-b-polyphosphate block-copolymer was used for the first time for the PNC preparation. The NDDSs were compared by their physicochemical characteristics, AG release, storage stability, stability in serum, complement consumption and toxicity against a human macrovascular endothelial cell line (EAhy926). The diameter and surface charge of the NDDSs were comparable with previously reported injectable nanocarriers. The NDDSs showed good encapsulation efficiency and drug loading. Moreover, the NDDSs were stable during storage and in fetal bovine serum for extended periods, showed low complement consumption and were non-toxic to EAhy926 cells up to high concentrations. Therefore, they can be considered as potential injectable nanocarriers of AG. Due to less pronounced burst effect and extended release characteristics, the nanocapsules could be favorable approaches for achieving prolonged pharmacological activity of AG using injectable NDDS.

1. Introduction

Apigenin (AG) is a natural plant flavonoid (4′, 5, 7,-trihydroxy-flavone), widely found in many common fruits and vegetables e.g. oranges, grapefruit, chamomile, tea, parsley, onions and wheat sprouts (Patel et al., 2007; Zheng et al., 2005). It showed a number of significant beneficial bioactivities i.e. anti-oxidant (Romanova et al., 2001), anti-inflammatory (Lee et al., 2007) and anti-cancer properties (Shukla and Gupta, 2010). Despite the numerous positive effects, AG is characterized by very low aqueous solubility

Abbreviations: AG, apigenin; AL-AG, apigenin loaded anionic liposome; AL-blank, empty anionic liposome; BCS, Biopharmaceutical Classification System; Chol, cholesterol; CL-AG, apigenin loaded cationic liposome; CL-blank, empty cationic liposome; DC-, dimethylaminoethane-carbamoyl chain; DC-Chol, 3ß-[*N*-(*N*′,*N*′-dimethylaminoethane)-carbamoyl]cholesterol hydrochloride; DLS, dynamic light scattering; DMEM, Dulbecco's modified Eagle's medium; DOPE, 1,2-dioleoyl-sn-glycero-3-phosphoethanolamine; DPPC, 1,2-dipalmitoyl-sn-glycero-3-phosphocholine; DSPE-mPEG$_{2000}$, 1,2-distearoyl-sn-glycero-3-phosphoethanolamine-*N*-[methoxy(polyethylene glycol)-2000] ammonium salt; EE, entrapment efficiency; FBS, fetal bovine serum; HEPES, 4-(2-hydroxyethyl)piperazine-1-ethanesulfonic acid; HPLC, high-performance liquid chromatography; Kolliphor® HS15, macrogol 15 hydroxystearate; Labrafac Lipophile WL1349, caprylic/capric triglycerides; LDH, lactate dehydrogenase; Lipoid S PC-3, hydrogenated phosphatidylcholine from soybean; LNC, lipid nanocapsule; LNC-AG, apigenin loaded lipid nanocapsule; LNC-blank, empty lipid nanocapsule; MPS, mononuclear phagocytic system; MWCO, molecular weight cut-off; NaCl, sodium chloride; NDDS, nanosized drug delivery system; NHS, normal human serum; NTA, nanoparticle tracking analysis; PDI, polydispersity index; PEG, poly(ethylene glycol); PNC, polymeric nanocapsule; PNC-AG, apigenin loaded polymeric nanocapsule; PNC-blank, empty polymeric nanocapsule; PS80, polysorbate 80; TEM, transmission electron microscopy; UPW, ultra-pure water.

* Corresponding author at: INSERM U1066, MIcro et Nanomédecines Translationnelles, IBS-CHU ANGERS, 4 rue Larrey, 49933 Angers Cedex 9, France.
E-mail addresses: reatul.karim@ulg.ac.be, reatulkarim@gmail.com (R. Karim).

http://dx.doi.org/10.1016/j.ijpharm.2017.04.064
0378-5173/

(1.35 μg/mL) and high permeability (log P value 2.87) (Li et al., 1997) and it is then a Biopharmaceutical Classification System (BCS) II molecule (Zhang et al., 2012). Taking these into account, the development of its injectable formulations, useful to overcome the constraint of low oral bioavailability, is challenging as AG is insoluble in most biocompatible solvents (Zhao et al., 2013). Therefore, use of AG for *in vivo* studies is limited.

One of the most interesting strategies to overcome this issue is to encapsulate the AG in nanosized drug delivery systems (NDDSs). NDDSs, also known as nanocarriers, are promising and versatile approach for delivery of hydrophobic drugs (Karim et al., 2017; Lainé et al., 2014) with several advantageous properties i.e. adaptable characteristics with easily modifiable surface, capacity to entrap large quantities of hydrophobic drug and protect it from degradation, improve bioavailability, release drug in a controlled manner over extended period, prolong plasma circulation half-life and increase pharmacological effects (Peer et al., 2007; Zhang et al., 2008). Moreover, they can be modified for site-specific drug delivery which reduce side-effects and improve the therapeutic window (Karim et al., 2016). Among various nanocarriers, liposome (Eavarone et al., 2000; Felgner and Ringold, 1989), lipid nanocapsule (LNC) (Allard et al., 2008; Lamprecht et al., 2002) and polymer-based nanocapsule (PNC) (De Melo et al., 2012; Mora-Huertas et al., 2010) have been widely studied. Although these nanocarriers can be generally considered as vesicular systems, their composition and morphology are significantly different from each other. Liposomes have structural similarities with cellular organelles and are made of phospholipid bilayer(s) surrounding an aqueous core. Due to their particular structure, liposomes are capable to encapsulate both lipophilic drugs (in the lipidic-bilayer (s)) and hydrophilic drugs (in the core). In comparison, PNCs have a solid polymer-shell surrounding an oily core, where lipophilic drugs are encapsulated. Structure of LNCs is a hybrid among PNCs and liposomes; characterized by an oily-liquid core surrounded by a solid lipid shell. All three NDDSs, i.e. liposome (Sharma et al., 1996), LNC (Zanotto-Filho et al., 2013) and PNC (Mora-Huertas et al., 2012) have been widely studied to improve the delivery of poorly water soluble drugs. Additionally, these nanocarriers can be designed for parenteral administration, in order to bypass absorption process and maximize the drug bioavailability. AG-loaded injectable NDDSs can be particularly beneficial for treatment of numerous types of cancers (e.g. colon cancer, brain cancer, breast cancer, liver cancer, prostate cancer, cervical cancer, thyroid cancer, skin cancer, gastric cancer etc.) due to the promising activity of AG [reviewed in detail by Patel et al., Shukla and Gupta] (Patel et al., 2007; Shukla and Gupta, 2010) and the capability of NDDSs to extravasate and preferentially accumulate in tumors by enhanced permeability and retention effect (Fu et al., 2009; Iyer et al., 2006). However, after administration into blood circulation, the NDDSs can be destabilized by plasma proteins leading to premature drug release. Moreover, they can form aggregates or adsorb a significant amount of plasma proteins and form a "protein-corona" (Palchetti et al., 2016). If opsonins are adsorbed on the surface, the NDDSs are subsequently captured and rapidly eliminated from the systemic circulation by mononuclear phagocytic system (MPS) (a part of the immune system) which restricts their blood circulation time. Formation of aggregates can also result rapid NDDS uptake by MPS (He et al., 2010). Therefore, stability of NDDSs in serum and low complement protein consumption are necessary for developing of safe and long-circulating nano-therapeutics for future clinical use (Li et al., 2015; Moore et al., 2015).

Different NDDSs are prepared from diverse ingredients and have variations in morphology, surface characteristics, drug loading capacity, drug release rates, toxicity etc. The purpose of this study was to develop and compare the characteristics of different injectable AG-NDDSs in order to identify the nanocarrier (s) that can deliver the largest quantity of AG while being biocompatible. Two liposomes with different surface characteristics (anionic and cationic), a LNC and a PNC were prepared. A novel block-copolymer i.e. tocopherol modified poly(ethylene glycol) (PEG)-b-polyphosphate (Fig. S1 in Supplementary material) (Vanslambrouck, 2015) was used for the first time for PNC preparation. Different techniques were used for preparation of the nanocarriers, and the so-obtained NDDSs were physicochemically characterized. Moreover, stability of the NDDSs in fetal bovine serum (FBS) and their complement protein consumption in normal human serum (NHS) were evaluated. Toxicity of the nanocarriers was assessed against a human macrovascular endothelial cell line to evaluate their biocompatibility.

2. Materials and methods

2.1. Materials

1,2-Dipalmitoyl-sn-glycero-3-phosphocholine (DPPC), 1,2-dioleoyl-sn-glycero-3-phosphoethanolamine (DOPE), 3ß-[*N*-(*N*′,*N*′-dimethylaminoethane)-carbamoyl]cholesterol hydrochloride (DC-Chol) and 1,2-distearoyl-sn-glycero-3-phosphoethanolamine-*N*-[methoxy(polyethylene glycol)-2000] ammonium salt (DSPE-mPEG$_{2000}$) were purchased from Avanti Polar Lipids, Inc. (USA). Cholesterol (Chol), 4-(2-hydroxyethyl)piperazine-1-ethanesulfonic acid (HEPES), sodium chloride (NaCl) and macrogol 15 hydroxystearate (Kolliphor® HS15) were purchased from Sigma-Aldrich (Germany). Hydrogenated phosphatidylcholine from soybean (Lipoid S PC-3) was provided from Lipoid GmbH (Germany), caprylic/capric triglycerides (Labrafac Lipophile WL1349) was supplied by Gattefosse (France). Polysorbate 80 (PS80) was purchased from Merck (Germany). AG was purchased from Indis NV (Belgium). The tocopherol modified PEG-b-polyphosphate copolymer (PEG$_{120}$-b-(PBP-co-Ptoco)$_9$) was synthesized by organocatalyzed ring-opening polymerization (Clement et al., 2012) of a butenylphosphate ring from a monomethoxy(polyethylene glycol) macroinitiator (MeO-PEG-OH, MW 5000 g/mol, Aldrich) (Yilmaz et al., 2016) followed by the grafting of a tocopherol derivative on the polyphosphate backbone by thiol-ene reaction (Baeten et al., 2016) (Fig. S1 in Supplementary material). Ultra-pure water (UPW) was obtained from a Millipore filtration system. All the other reagents and chemicals were of analytical grade. Normal human serum (NHS) was provided by the "Etablissement Français du Sang" (Angers, France). Sheep erythrocytes and hemolysin were purchased from Eurobio (France). EAhy926 cells (human umbilical endothelial cell line), Penicillin-Streptomycin, and Dulbecco's modified Eagle's medium (DMEM) were provided by Lonza (Belgium). Fetal bovine serum (FBS) was provided by Biologicals Industries (USA).

2.2. Preparation of NDDSs

2.2.1. Preparation of cationic liposomes and anionic liposomes

The cationic and anionic liposome formulations (CL-AG and AL-AG respectively, composition shown in Table 1, CL composition is modified from (Bellavance et al., 2010)) were prepared by thin lipid-film hydration, extrusion (Wei et al., 2015) and PEG post-insertion method. Briefly, AG and the excipients were dissolved in absolute ethanol and then dried in a rotary evaporator at 30 °C for 1 h to form a dry lipid film. Subsequently, the dried film was hydrated with HEPES buffer (pH 7.4) and hardly agitated for 15 min. Afterwards, the lipid dispersion was extruded consecutively through 0.4 μm (3×), 0.2 μm (3×) and 0.1 μm (3×) polycarbonate membranes (Nucleopore®, Whatman) at 50 °C (above phase transition temperature of DPPC) to obtain primary liposomes.

DSPE-mPEG$_{2000}$ (in HEPES buffer) was added to the surface of the primary liposomes by post-insertion technique, by incubation at 50 °C for 30 min. The liposome formulations were then purified by dialysis (MWCO 20 kD, Spectra/Por® biotech grade cellulose ester membrane, SpectrumLabs, Netherlands) against HEPES buffer (pH 7.4) at 4 °C for 2 × 1 h cycles.

Blank liposomes (CL-blank and AL-blank) were prepared following the same procedure but without the addition of AG.

2.2.2. Preparation of lipid nanocapsules

The apigenin-loaded LNCs (LNC-AG) were prepared using phase inversion temperature technique (Laine et al., 2014). In brief, AG (0.2% w/w), Kolliphor® HS15 (16.5% w/w), Lipoid® S PC-3 (1.5% w/w), Labrafac Lipophile WL1349 (20.1% w/w), DSPE-mPEG$_{2000}$ (1.9% w/w), NaCl (1.7% w/w) and UPW (58% w/w) were mixed under magnetic stirring at 60 °C. Three heating-cooling cycles were performed between 90 °C and 60 °C. During the last cooling step, when the temperature was in the phase inversion zone (78–83 °C), ice-cold UPW was added (final concentration 69.8% w/w) to induce irreversible shock and form the LNC-AG. The nanocapsules were then diluted with HEPES buffer and passed through 0.2 μm cellulose acetate filter to remove any aggregates. Purification was done by dialysis method as described in 2.2.1.

Blank LNCs (LNC-blank) were prepared by the same procedure as LNC-AG, but without the addition of AG.

2.2.3. Preparation of polymer-based nanocapsules

The apigenin-loaded PNCs (PNC-AG) were prepared using nanoprecipitation technique followed by solvent evaporation under vacuum (Mora-Huertas et al., 2012). In short, AG (1.2% w/w), PEG$_{120}$-b-(PBP-co-Ptoco)$_9$ (20.1% w/w), Lipoid® S PC-3 (10.8% w/w), Labrafac Lipophile WL1349 (67.9% w/w) were dissolved in ethanol:acetone (1:3 v/v). Subsequently, the solution was slowly injected (0.8 mm needle) into an aqueous solution of PS80 (0.25% w/v) under magnetic stirring at 400 rpm. After 10 min stirring, the organic solvent was completely removed by evaporation under reduced pressure at 40 °C. The PNC-AG was purified by dialysis method as described in 2.2.1.

Blank PNCs (PNC-blank) were prepared in the same procedure as PNC-AG, but without the addition of AG.

2.3. Size distribution, zeta-potential and morphology

The mean diameter and polydispersity index (PDI) of the NDDSs were determined by dynamic light scattering (DLS) technique using Zetasizer Nano ZS (Malvern Instruments Ltd, UK). NDDSs were diluted 100-folds in UPW before the analysis. The measurements were performed at backscatter angle of 173°. The measured average values were calculated from 3 runs, with 10 measurements within each run.

Additionally, the size distribution of the NDDSs was determined using nanoparticle tracking analysis (NTA), which complements the DLS measurements. The NTA was carried out using the NanoSight NS300 (Malvern Instruments Ltd, UK). Briefly, the NDDS samples were diluted to optimum concentrations with UPW and were infused in the sample chamber using a syringe pump at 30 μL/min rate. A 405 nm laser was used to illuminate the particles, and their Brownian motion was recorded into three 60 s videos (25 fps) using the sCMOS type camera of the instrument. Subsequently, the NTA software (NTA 3.2 Dev Build 3.2.16) analyzed the recordings, tracked the motion of the particles and calculated the diameter of the particles. The experiment was performed in triplicate.

Zeta potential of the nanocarriers was measured using laser Doppler micro-electrophoresis technique using Zetasizer Nano ZS (Malvern Instruments Ltd, UK).

Morphology and size of the NDDSs were visualized by transmission electron microscopy (TEM) using negative staining technique. Briefly, a drop of the NDDS dispersion was placed for 30 s on a TEM copper grid (300 mesh) with a carbon support film. The excess dispersion was removed with a filter paper. Subsequently, staining was done by adding a drop of 1% (w/v) aqueous solution of uranyl acetate on the grid for 1.5 min, followed by removal of excess solution. The TEM observations were carried out with a JEOL JEM-1400 transmission electron microscope equipped with a Morada camera at 100 kV.

Table 1
Molar ratio of ingredients of CL-AG and AL-AG.

Ingredient	Molar ratio	
	CL-AG	AL-AG
DPPC	1	1
DC-Chol	0.77	–
Chol	–	0.77
DOPE	0.77	0.77
DSPE-mPEG$_{2000}$ (during dry lipid film formation)	0.01	0.01
DSPE-mPEG$_{2000}$ (post insertion)	0.04	0.04
AG	0.13	0.13

2.4. Apigenin dosage via HPLC method

To quantify total (encapsulated and unencapsulated) AG concentration, CL-AG, AL-AG, and LNC-AG were broken by mixing vigorously with an appropriate volume (7-folds dilution for CL-AG and AL-AG, 40-folds dilution for LNC-AG) for of ethanol to keep dissolved AG concentration between 5 and 50 μg/mL. PNC-AG was processed in the similar way, except ethanol:acetone (1:3 v/v, 7-folds dilution) was used as the solvent. To quantify unencapsulated AG concentration, formulations were placed on centrifugal concentrator devices with polyethersulfone membrane (MWCO 30 kD, Vivaspin 500, Sartorius AG) and centrifuged at 14500*g* for 20 min to separate the free AG from the rest of the formulation. The filtrates containing unencapsulated AG were collected and ethanol (2-folds) was added to solubilize any undissolved drug. AG dosage in the above mentioned samples was performed by a validated method in a HPLC system (LC Agilent 1100 series, Agilent Technologies, Belgium). An Alltima™ HP C18 analytical column (250 × 4.6 mm, 5 μm, Grace Divison Discovery Sciences, Belgium) was used at 30° C. UPW and acetonitrile (55:45, v/v) was used as mobile phase. Flow rate was 1 mL/min, injection volume was 10 μL and AG was quantified by an UV detector at λ of 340 nm. Analysis of the data was performed by Open Lab HPLC Agilent software. Retention time for AG was 4.9 min.

2.5. Entrapment efficiency (EE)

$$\mathrm{EE}(\%) = \frac{(\text{Total AG conc. in NDDS} - \text{unencapsulated AG conc. in NDDS}) * \times 100}{\text{Theoritical AG conc. in NDDS}}$$

*Determined by HPLC (2.4)

2.6. Mass yield and drug loading capacity

Mass yield of NDDSs was calculated by gravimetric analysis of the dried NDDSs dispersions. Briefly, 200 μL of NDDSs were freeze-dried (Drywinner 8, Heto-Holten A/S, Denmark) over a 24 h cycle. Weight of the dried nanocarriers were measured (weights of HEPES buffer and NaCl were taken into account) and mass yield (%)

was calculated using the following equation:

$$\text{Mass yield}(\%) = \frac{\text{Weight of 200 } \mu\text{L NDDS} \times 100}{\text{Theoretical weight of 200 } \mu\text{L NDDS}}$$

Drug loading capacity was calculated using the following equation:

$$\text{Drug loading capacity}\left(\frac{\mu\text{g AG}}{\text{mg NDDS}}\right) = \frac{\text{Amount of AG in 200 } \mu\text{L NDDS} * (\mu\text{g})}{\text{Weight of 200 } \mu\text{L NDDS(mg)}}$$

*Determined by HPLC (2.4)

2.7. In vitro *drug release profile of the NDDSs*

In vitro drug release profiles of the nanocarriers were studied with the dialysis method. In brief, 1 mL of AG loaded NDDSs were taken in a dialysis bag (MWCO 20 kD, Spectra/Por® biotech grade cellulose ester membrane, SpectrumLabs, Netherlands) and dialyzed against HEPES buffer (pH 7.4) (200/1 acceptor/donator volume ratio to obtain sink condition) at 37° C, stirred at 75 rpm (SW22, Julabo GmbH, Germany). The concentration of AG was determined by HPLC method described in 2.4.

2.8. Storage stability

The NDDSs were kept at 4 °C and samples were withdrawn at day 0, 1, 3, 7 and 14. Stability during storage was evaluated by size, PDI (using method described in 2.3), AG content (using HPLC method described in 2.4) and AG leakage. The leakage of AG from NDDSs was assessed using the method to quantify unencapsulated AG mentioned in Section 2.4.

2.9. Stability of the NDDSs in serum

Stability of the NDDSs in FBS was evaluated by following their size distribution against time (Li et al., 2015; Palchetti et al., 2016). The nanocarrier formulations were diluted using HEPES buffer (pH 7.4) to optimum concentrations (200 μg lipid/mL for CL-AG, AL-AG and PNC-AG; 500 μg lipid/mL for LNC-AG) and mixed with FBS at 1:1 ratio (v/v) at 37° C. The mixture, along with nanocarrier dispersion and FBS (controls), were incubated at 37° C at 75 rpm in a shaking water bath (SW22, Julabo GmbH, Germany). At predetermined time intervals (1 min, 30 min, 1 h, 2 h, 4 h, 6 h and 24 h), 20 μL of samples were withdrawn, diluted 50-folds with UPW and size distribution was measured via DLS method described in 2.3.

2.10. Complement consumption by the NDDSs

Complement activation was evaluated by measuring the residual hemolytic capacity of NHS towards antibody-sensitized sheep erythrocytes after exposure to the different NDDSs (CH50 assay) (Cajot et al., 2011). In brief, aliquots of NHS were incubated with increasing concentrations of the NDDSs at 37 °C for 1 h. Subsequently, the different volumes of the NHS were incubated with a fixed volume of hemolysin-sensitized sheep erythrocytes at 37 °C for 45 min. The volume of serum that can lyse 50% of the erythrocytes was calculated ("CH50 units") for each sample and percentage of CH50 unit consumption relative to negative control was determined as described previously (Vonarbourg et al., 2006). Particle number in the NDDS dispersions was determined by NTA described in Section 2.3 and particle concentration per mL of NHS was calculated according to following equation-

$$\text{Particle number per mL of NHS} = \text{Particle conc. in NDDS dispersion} \times \frac{\text{vol. of NDDS added}}{\text{vol. of NHS}}$$

Subsequently, surface area of the NDDSs per mL of NHS was calculated according to the following equation-

$$\text{Surface area} = \text{Particle number per mL of NHS} \times \pi \times (\text{average particle diameter})^2$$

The CH50 unit consumption by the different NDDSs were compared by plotting the percentage of CH50 unit consumption as a function of their surface area.

2.11. In vitro *cytotoxicity of NDDSs on endothelial cell line*

The endothelial cells (EAhy926) were seeded in a 96-well plate at a density of 12.5×10^3 cells/well and incubated for 24 h. AG solution (in DMSO) and NDDSs, at a concentration of 0.6 μM to 40 μM, were added to the cells in 200 μL of cell media and incubated for 24 h. Cytotoxicity of formulations was determined by evaluating cell viability using methyl tetrazolium (MTS) assay (CellTiter 96® Aqueous One Solution Cell Proliferation Assay, Promega, WI, USA) and cell necrosis by lactate dehydrogenase (LDH) assay (Cytotoxicity Detection Kit^{PLUS}, Roche, Basel, Switzerland), according to manufacturer's instructions.

2.12. Statistical analysis

Results obtained from the experiments were analyzed statistically using GraphPad Prism® software. Mean and standard deviation (SD) were determined and values are represented as Mean ± SD. One way analysis of variance (ANOVA) was performed in the respective fields with Bonferroni post-test to compare among individual groups, and Dunnett's post-test to compare with control. P-value less than 0.05 ($p < 0.05$) was considered to be statistically significant.

3. Results

3.1. Characteristics of the NDDSs

Particle size and zeta potential of the developed NDDSs (determined by DLS) are shown in Table 2. The mean hydrodynamic diameter of the AG loaded liposomes (CL-AG and AL-AG) and the PNC-AG was comparable ($p > 0.5$). The sizes of these nanocarriers were around 143 nm. The mean diameter of the LNC-AG was significantly ($p < 0.001$) smaller (59 nm) compared to the other

Table 2
Physicochemical characteristics of the NDDSs.

Characteristics	CL-AG	AL-AG	LNC-AG	PNC-AG
Mean diameter (nm)[a]	144 ± 1	142 ± 6	59 ± 2	145 ± 7
PDI	0.04 ± 0.01	0.12 ± 0.02	0.11 ± 0.03	0.11 ± 0.02
Zeta potential (mV)	43.2 ± 1.2	−27.4 ± 2.3	−24.9 ± 6.0	−16.2 ± 4.4
EE (%)	71 ± 2	34 ± 1	82 ± 5	84 ± 4
Mass yield (%)	80 ± 3	86 ± 5	72 ± 2	81 ± 4
Drug loading capacity (μgAG/mgNDDS)	16.5 ± 0.2	6.5 ± 0.3	6.2 ± 0.5	14.3 ± 0.6

[a] Measured by DLS.

NDDSs. All four NDDSs were monodispersed with PDI <0.2. The mean diameter of the CL-AG, AL-AG, LNC-AG and PNC-AG determined by NTA analysis were 133 nm, 136 nm, 54 nm and 141 nm respectively. This was in agreement with the results obtained from DLS. Morphology of the NDDSs was visualized by TEM images (Fig. 1). The NDDSs were nearly spherical and the liposomes were unilamellar. Additionally, mean sizes of CL-AG, AL-AG, LNC-AG and PNC-AG determined by TEM were 111 nm, 214 nm, 55 nm and 87 nm respectively. Mean size (determined by TEM) of CL-AG and LNC-AG were comparable with the results obtained by DLS and NTA, whereas average size of AL-AG and PNC-AG were quite dissimilar. This can possibly occur due to the differences of the physical state of the samples (dry vs hydrated state) and size calculation techniques of TEM compared to DLS (number vs intensity weighted).

The zeta potential of the CL-AG was 43.2 mV and was significantly different ($p < 0.001$) compared to the other NDDSs, which were negatively charged. Surface charge of AL-AG, LNC-AG and PNC-AG were −27.4 mV, −24.9 mV and −16.2 mV respectively. However, only the zeta potentials of AL-AG and PNC-AG were significantly different ($p < 0.05$) among these three NDDSs.

EE of the CL-AG was 71% which was significantly higher ($p < 0.001$) compared to the AL-AG. Moreover, EE of the nanocapsules were significantly higher compared to the CL-AG ($p < 0.05$) and AL-AG ($p < 0.001$) but were comparable ($p > 0.05$) with each other (82% for LNC-AG and 84% for PNC-AG).

Mass yields of the NDDSs were between 72 and 85%. The highest yield mass was observed for AL-AG, followed by LNC-AG, PNC-AG and CL-AG. No significant difference ($p > 0.05$) was observed for yield mass of CL-AG and PNC-AG. Drug loading capacity in CL-AG and PNC-AG were more than 2-fold higher (16.5 and 14.3 μgAG/mgNDDS respectively) compared to AL-AG and LNC-AG (6.5 and 6.2 μgAG/mgNDDS respectively). Drug loading capacity of the NDDSs were significantly different ($p < 0.01$) from each other, except for AL-AG and LNC-AG.

3.2. In vitro *drug release profile of the NDDSs*

The drug release (%) from the NDDSs was plotted against time to obtain their drug release profiles (Fig. 2). Faster release profiles were observed for the liposomes in comparison to the nanocapsules. Although initial release from CL-AGs was slower compared to the AL-AGs, the liposomes released about 85–91% drug after 6 h.

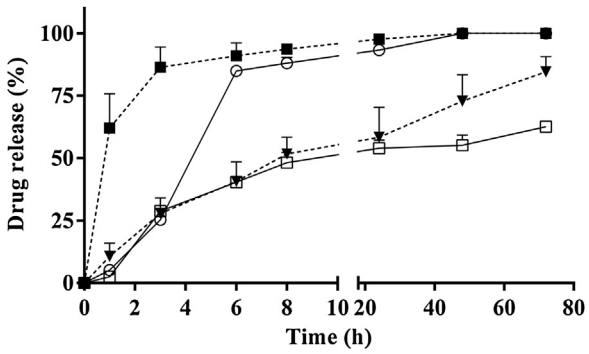

Fig. 2. *In vitro* drug release from CL-AG (○), AL-AG (■), LNC-AG (□) and PNC-AG (▼).

In comparison, the nanocapsules showed a biphasic and more sustained release profile, with a faster release rate up to 8 h, followed by a much slower rate up to 72 h. Moreover, the release rates of LNC-AG and PNC-AG were very comparable up to 24 h, with a release of 54% and 58% drug respectively. However, the drug release rate of PNC-AG was relatively quicker after 24 h compared to LNC-AG. After 72 h, the LNC-AG released 63% drug whereas PNC-AG released 85% drug.

3.3. Storage stability of the NDDSs

Stability of the NDDSs during storage was evaluated using several parameters i.e. size distribution (mean diameter and PDI), AG concentration and drug leakage. Mean size and PDI were determined to evaluate the physical stability of the nanocarriers, AG concentration will provide information about chemical stability of the drug within the NDDSs, whereas drug leakage will give evidence of the robustness of the NDDSs during storage. Size of all four NDDSs were stable throughout the study period (Fig. 3a).

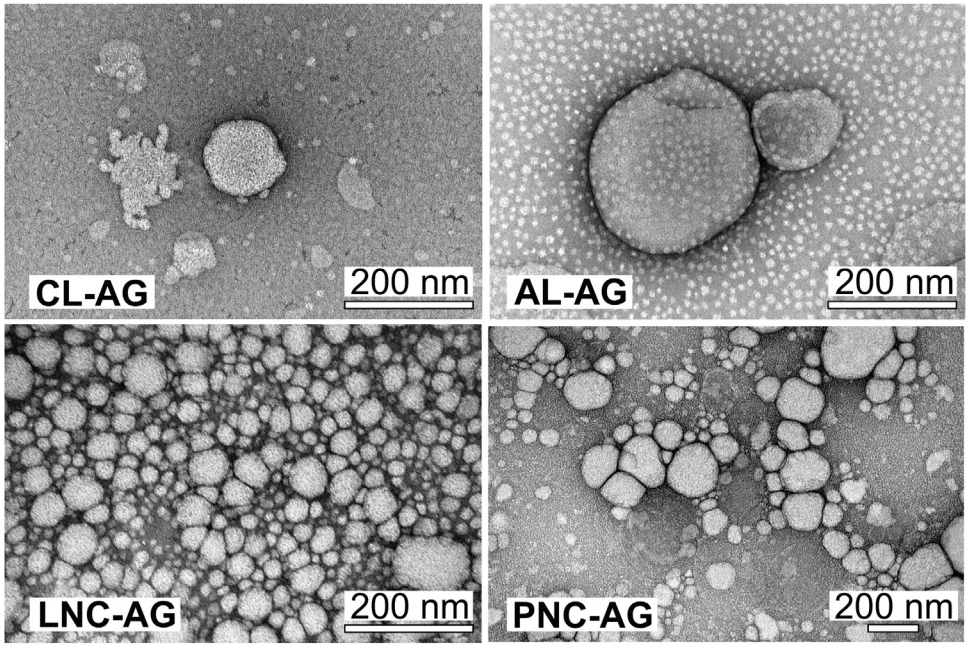

Fig. 1. Representative transmission electron microscopy images of CL-AG, AL-AG, LNC-AG and PNC-AG (white bar: 200 nm).

Moreover, PDI of the nanocarriers were below 0.2 up to 14 days showing that the formulations remained monodispersed.

AG concentrations (% of initial) in the nanocarriers are showed in Fig. 3b. The AG% in AL-AG, LNC-AG and PNC-AG remained unaffected, signifying the stability of the drug in these nanocarriers. However, AG% in CL-AGs gradually reduced to 90% of initial concentration after 14 days, demonstrating possible drug degradation in this NDDS. No drug leakage from any of the NDDSs was observed up to 14 days.

3.4. Stability of the NDDSs in serum

Stability of the NDDSs in serum was evaluated by following their size distribution in FBS (at 37 °C, 75 rpm) against time using DLS in order to detect any alteration in their diameter and to determine possible particle destabilization, aggregation or protein corona formation. Additionally, the NDDS dispersions and FBS were also incubated under same conditions as controls.

As DLS shows size distribution graphs in relative intensity (%), the height of an unimodal peak will be higher compared to the same peak in a mixed multimodal sample. Moreover, focusing a particular size range (e.g. 0–50 nm or 100–300 nm) and getting information about a specific peak from a mixture is not possible in DLS. Therefore, peak heights of NDDS-FBS mixtures were normalized in the overlaid size graphs (FBS, NDDS, NDDS +FBS) (Fig. 4a) for easier qualitative comparison with the controls, while position of the normalized peaks still provided information about possible corona formation.

Throughout the study period, size distributions of the control NDDSs were unimodal and their diameter did not change (Fig. 4). Therefore, no signs of particle aggregation or degradation were observed. Size distribution of the control FBS remained bimodal (more frequent, peaks around 10–15 nm and 30–50 nm) or trimodal (less frequent additional small peak around 200 nm) up to 6 h of the study. However, larger aggregates were often observed in control FBS after 24 h with peaks around 300–500 nm.

Up to 6 h, size distributions of the NDDS-FBS mixtures for CL-AG, AL-AG and PNC-AG were trimodal, showing the peaks of the free proteins (around 10–15 nm and 30–50 nm) and the NDDSs (peaks around 120–150 nm). Position of the peaks of NDDS-FBS mixtures were comparable with the corresponding control peaks. However, size distribution graph for LNC-AG-FBS mixture was bimodal as one of the peaks (around 30–50 nm) of FBS overlapped with the peak of LNC-AG, resulting a wider combined peak instead of two separate peaks. Moreover, higher concentration of LNC-AG was necessary, compared to CL-AG, AL-AG and PNC-AG, to observe its peaks in FBS due to the overlapping peaks. However, the peak of the NDDS was identifiable due to the increased height of the second peak in the LNC-AG-FBS mixture. The position of LNC-AG-FBS peaks were comparable with the controls (LNC-AG and FBS), like the other NDDSs. Therefore, up to 6 h, none of the NDDSs showed any signs of particle aggregation or adsorbing large amount of serum proteins, demonstrating their colloidal stability in serum.

The respective peaks of CL-AG, AL-AG and LNC-AG in FBS shifted toward larger diameters after 24 h. However, it is difficult to come into conclusion that the augmentation of diameter is due to protein adsorption and corona formation around the NDDS surface, or due to particle aggregation as the control FBS showed aggregated particle peaks around 300–500 nm after 24 h. However, in the experiment with PNC-AG, the NDDS peak in FBS mixture did not shift toward higher value after 24 h, and the control FBS also did not show any peaks of large aggregated particles.

3.5. Complement consumption by the NDDSs

The complement consumption by the different NDDSs were measured by CH50 assay. Their percentage of CH50 unit consumption was plotted as a function of the particle surface area per mL of NHS (Fig. 5). As usually observed, the complement consumption for the four nanocarriers was increasing with the amount of NDDS added in NHS. The LNC-AG showed the lowest CH50 consumption and reached only 2.1% at 800 cm^2/mL of NHS. The complement consumption of AL-AG and CL-AG increased gradually and reached 17.5% at 852 cm^2/mL of NHS and 26.8% at 752 cm^2/mL of NHS respectively. Although the PNC-AG consumed higher CH50 units at smaller surface areas than the others, its consumption increased slowly when more nanoparticles were added and reached 23.7% at 838 cm^2/mL of NHS.

3.6. In vitro *cytotoxicity of the NDDSs on endothelial cells*

Cytotoxicity of AG solution and the NDDSs on EAhy926, a human endothelial cell line, was evaluated *in vitro* by two different assays i.e. MTS and LDH assay (Fig. 6). The drug solution did not show any significant toxicity in both assays. The CL-AG and CL-blank showed no signs of toxicity up to 2.5 μM. However, significant reduction of cell viability was revealed at concentrations ≥10 μM, corresponding to ≥171 μg/mL of CL-AG (Table 3). Correspondingly, significant necrosis was observed in LDH assay at similar concentrations of CL-blank and PNC-blank. However, the AL-blank, AL-AG, LNC-blank, LNC-AG and PNC-AG showed no significant reduction in cell viability or any substantial cell necrosis at the test concentrations. Overall, the results observed in MTT and LDH assays were comparable and the nanocarriers were nontoxic

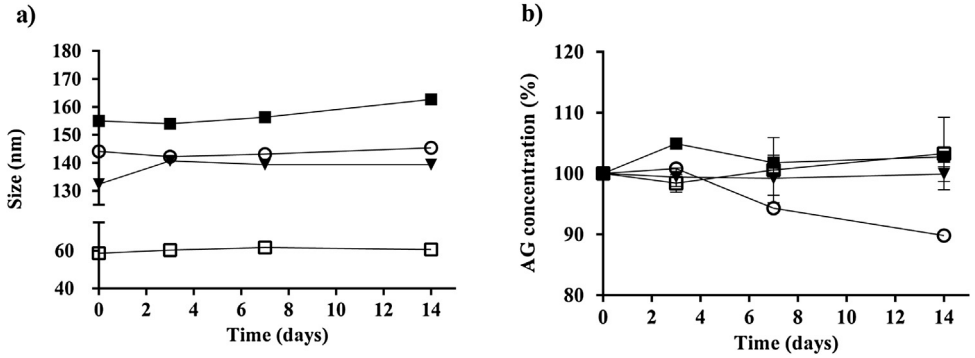

Fig. 3. Stability profiles of the NDDSs at 4 °C up to 14 days: a) Mean diameter of CL-AG (○), AL-AG (■), LNC-AG (□) and PNC-AG (▼) at 4 °C up to 14 days; b) Apigenin concentration (% of day 0) in CL-AG (○), AL-AG (■), LNC-AG (□) and PNC-AG (▼).

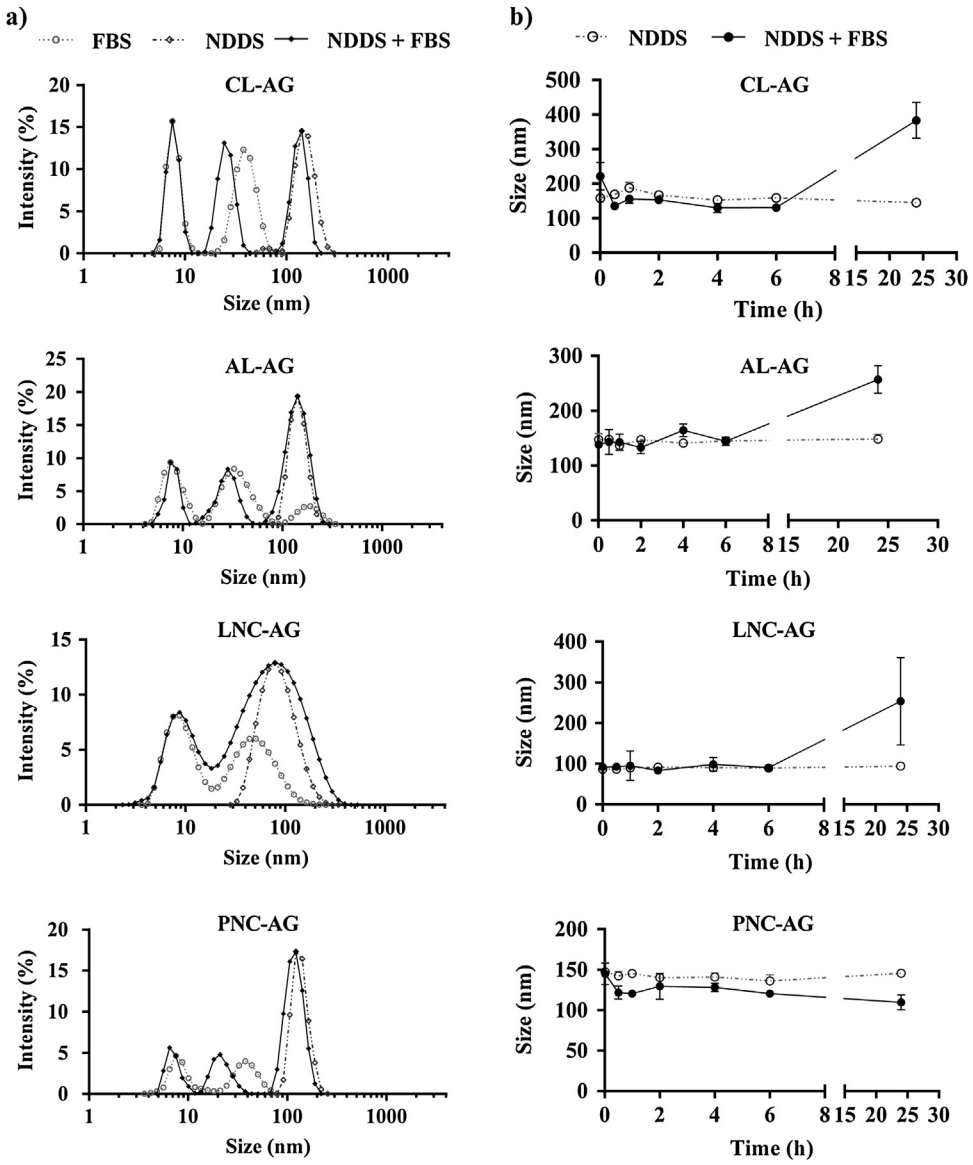

Fig. 4. a) Size distribution profiles of CL-AG, AL-AG, LNC-AG and PNC-AG in FBS at 37° C and 75 rpm after 6 h. b) Diameter of CL-AG, AL-AG, LNC-AG and PNC-AG in FBS at 37° C and 75 rpm up to 24 h.

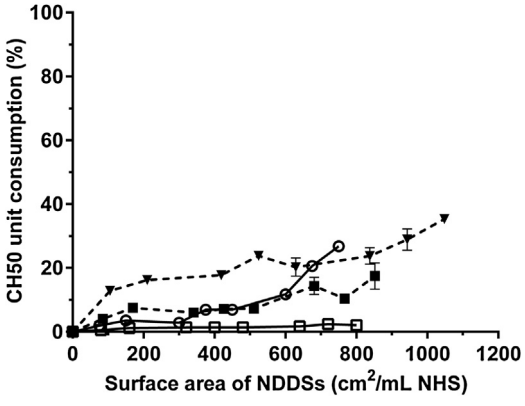

Fig. 5. Complement consumption at 37 °C by CL-AG (○), AL-AG (■), LNC-AG (□) and PNC-AG (▼).

up to high concentrations of the NDDSs (AG conc. and corresponding NDDS conc. are shown in Table 3).

4. Discussion

The aim of the present study was to develop injectable dosage forms of AG, to allow their use for *in vivo* studies. AG showed many promising pharmacological activities, but its *in vivo* use is restricted due to very low aqueous solubility. As a result, very slow dissolution would occur after oral administration, which is the rate limiting step causing slow absorption and low bioavailability (Zhang et al., 2013). In fact, a study on pharmacokinetics and metabolism of AG reported that the drug reached the systemic circulation 24 h after oral administration (Gradolatto et al., 2005). Parenteral administration of AG solution formulations can overcome the problem of bioavailability, but face challenges of short plasma half-life (90–105 min) (Wan et al., 2007; Zhang et al., 2013) and nonspecific high tissue distribution (Wan et al., 2007). Moreover, rapid crystallization may occur when these formulations are injected into blood which reduces its availability at

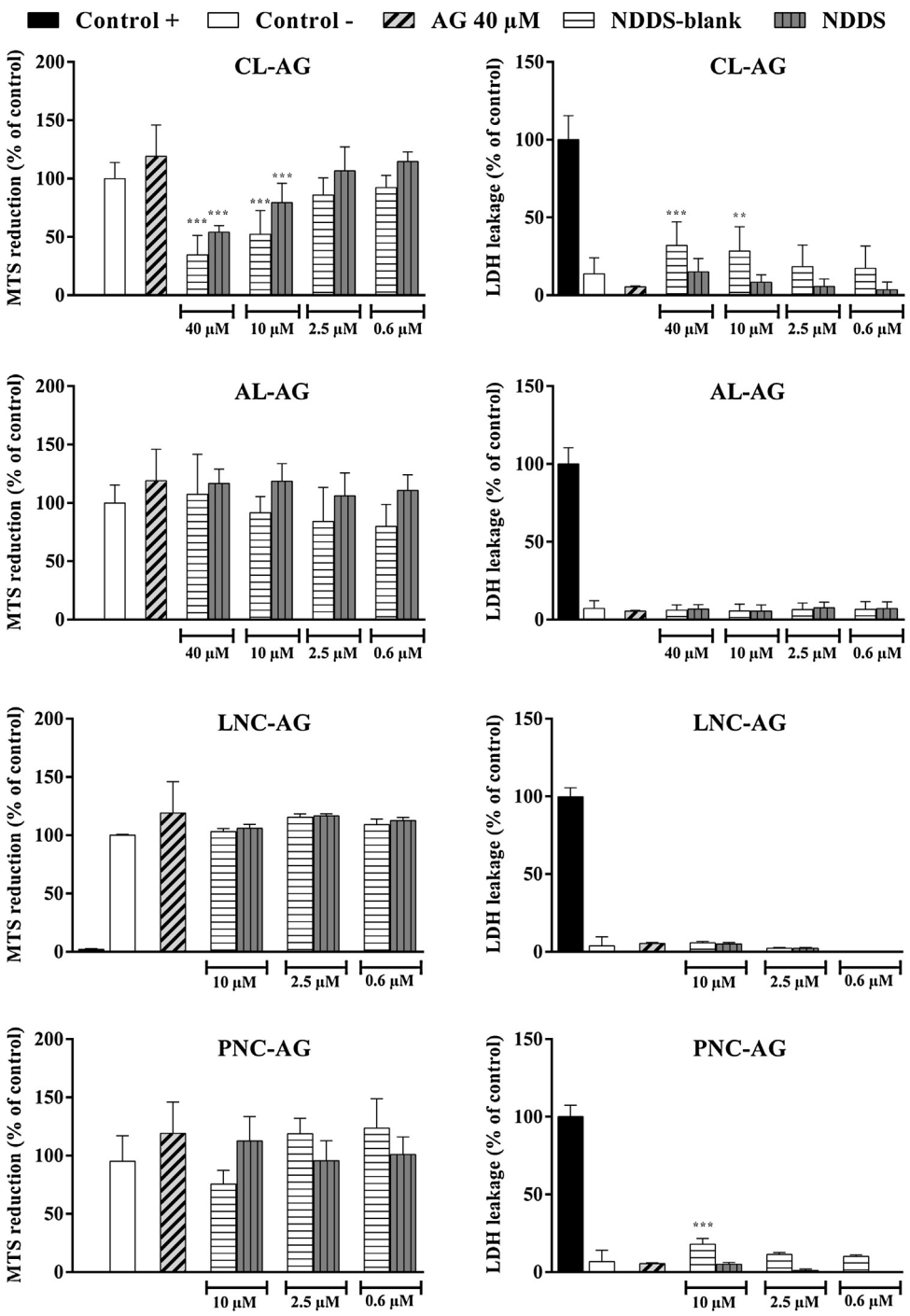

Fig. 6. Cytotoxicity of AG, CL-AG, CL-blank, AL-AG, AL-blank, LNC-AG, LNC-blank, PNC-AG and PNC-blank on EAhy926 cells. The cells were treated for 24 h. At the end of the incubation period, cell viability was determined by the MTS reduction assay and cell necrosis was quantified by LDH assay, as described in Section 2.11. (Oneway ANOVA with Dunnett's post-test. $p < 0.1$ is denoted by (*), $p < 0.01$ by (**) and $p < 0.001$ by (***)).

Table 3
AG concentrations and corresponding NDDS concentrations.

AG conc. (μM)	Corresponding NDDS concentration (μg/ml)			
	CL-AG	AL-AG	LNC-AG	PNC-AG
40.0	683	1678	1744	756
10.0	171	420	436	189
2.5	43	105	109	47
0.6	10	25	26	11

diseased tissue (Engelmann et al., 2002). In fact, Engelmann et al. observed enlarged abdominal lymph nodes in mice caused by AG deposition after treatment with such formulation of the drug (Engelmann et al., 2002). Hence, it is necessary to develop suitable drug carrier systems for AG with sufficient stability during storage and in serum. Therefore, three types of NDDSs of AG were developed in this study i.e. liposomes, LNC and PNC; and were evaluated as potential injectable formulations of AG. For PNC

preparation, a novel tocopherol modified PEG-b-polyphosphate block-copolymer was used for the first time. The amphiphilic surface active properties of the polymer can aid to improve nanocarrier stability which has been already described in the literature (Lopalco et al., 2015). The use of polyphosphate backbone instead of commonly utilized polylactide or polyglycolide chains is more biocompatible as the degradation products of polyphosphates do not create extreme acidic environment (Yilmaz and Jerome, 2016). The presence of tocopherol on the polyphosphate chain helps to improve entrapment of hydrophobic drugs like AG (Tripodo et al., 2015). Additionally, it may improve the stability of AG by acting as an antioxidant and protecting its phenol groups from oxidation.

Three key physicochemical properties of the nanocarriers influence their *in vivo* behavior: particle size, surface charge and surface coating (Straubinger et al., 1993). These properties must be optimized in order to achieve favorable drug delivery. Particle size is an important parameter which has profound impact on the uptake of NDDSs by MPS. The rate of MPS uptake increases as size of NDDSs increases (Senior et al., 1985). Size of the CL-AG, AL-AG and PNC-AG were comparable, but the LNC-AG had smaller diameter. Compared to AL-AG, the lipid bilayer of CL-AG had an additional dimethylaminoethane-carbamoyl (DC-) chain on cholesterol molecules which imparted a significant positive surface charge (as ionically bonded chloride ion dissociates from the hydrochloride salt of tertiary amine group of the DC- chain in aqueous environment) without affecting vesicle size. Although most components of the nanocapsule structures of the LNC-AG and PNC-AG were similar, the ratio of the excipients and manufacturing techniques were different, resulting in nanocapsules with dissimilar sizes. However, the major factor governing the higher size of the PNC-AG is possibly its higher weight fraction of core-oil (69%) compared to LNC-AG (50%), which is in accordance with previous reports (Heurtault et al., 2003; Lertsutthiwong et al., 2008). Though, size of all the NDDSs were within acceptable limits and comparable with previously studied systemically administered nanocarriers (Fu et al., 2009; Laine et al., 2014; Lim et al., 2015; Mosqueira et al., 2001).

The surface charge of nanocarriers is another critical parameter that is important from two perspectives- storage stability and *in vivo* distribution. Charged NDDSs are less prone to particle aggregation and more stable as dispersions, compared to neutral nanocolloids. Moreover, their cellular-interaction capacity and possibility of intracellular drug delivery are generally higher, compared to neutral NDDSs. Macrophage engulfment of charged nanocarriers increases as intensity of surface charge amplifies, whereas non-phagocytic cellular uptake increases the charge moves towards comparatively more positive value (He et al., 2010). The surface charges of the AG-loaded NDDSs can be ordered as follows- CL-AG > PNC-AG > LNC-AG $\geq$ AL-AG, where zeta potential of only CL-AG was positive.

The presence of additional DC- chain on the cholesterol of the lipid bilayer of CL-AG not only altered the zeta potential, but improved the EE by 2 folds, compared to AL-AG. This is possibly due to charged interaction between AG and the DC- chain. AG is a weakly acidic molecule having two pKa values (6.6 and 9.3) (Favaro et al., 2007), and therefore will be partially deprotonated at the pH of the buffer (7.4) with an equilibrium between mono-anionic and neutral species (Papay et al., 2016; Tungjai et al., 2008). Therefore, the neutral species can be entrapped in the lipid bilayer and the mono-anionic species can interact with the positively charged DC-chain on the CL-AG surfaces, resulting significantly improved drug entrapment. Yuan et al. observed similar electrostatic and/or hydrogen bond formation among AG and positively charged human serum albumin (Yuan et al., 2007). Additionally, Papay et al. reported probable electrostatic repulsion among AG and sulfobutylether-β-cyclodextrin, due to presence of negatively charged sulfo group in the cyclodextrin which weakened their complexation as pH was increased (Papay et al., 2016). Moreover, the ionized DC- chain is present both at the inner and outer surfaces of the lipid bilayer facing towards the aqueous core and the surrounding aqueous environment respectively. As AG was added during the formation of dry lipid film, we hypothesize that AG might be electrostatically attached with both inner and outer surfaces during formation of the liposome. The phenomenon is more evident from the drug release characteristics and storage stability (chemical) of CL-AG which is explained in the respective parts of the discussion. The nanocapsules had high EE which can be possibly attributed to the presence of an oily core.

Drug loading capacity of the CL-AG was 2.5 folds higher compared to AL-AG, due to the presence of the additional positively charged DC- chain. Similarly, drug loading capacity of PNC-AG was 2.3 folds more compared to LNC-AG, possibly due to presence of higher% of core oil in its formulation (Lertsutthiwong et al., 2008).

A major parameter evaluated in this study was the drug release characteristics of the different NDDSs, to determine their feasibility as extended release carriers of AG. In previous experiments, plasma concentration of AG was high after intravenous administration, but it rapidly fell with a half-life around 1.75 h (Wan et al., 2007), which can be due to either crystallization of apigenin in physiological pH (Engelmann et al., 2002), or formation of its metabolites (Gradolatto et al., 2004). To prolong the pharmacological activity, dosage forms having prolonged plasma circulation time and extended release profile can be beneficial. Drug release at 37 °C in HEPES buffer (pH 7.4, 285–295 mOsm/kg) from the liposomes was more rapid compared to the nanocapsules, which can be attributed to the different composition and morphology of the two types of nanocarriers. The nanocapsules have an oily core surrounded by hydrophobic and amphiphilic polymers. Therefore, majority of hydrophobic drugs like AG will be encapsulated in the core of such nanocarriers. However, liposomes entrap majority of AG within their lipid bilayer and thus released the drug more easily compared to nanocapsules. The release rate from CL-AG was comparatively slower than AL-AG, which can be attributed to two possible reasons. Firstly, the possible electrostatic attraction of AG with the positively charged DC- chain can hinder the movement of the drug from the lipid bilayer. Secondly, the likelihood of presence of a portion of the entrapped AG at the inner surface of the lipid bilayer of CL-AG (as some DC- chains will be present at that surface) which provides more obstacles in the movement pathway of the drug. However, the nanocapsules i.e. LNC-AG and PNC-AG showed much sustained release characteristics than the liposomes. The release rate of the nanocapsules was comparable up to 24 h, but the PNC-AG showed slightly faster release rate afterwards, compared to LNC-AG. The higher% of excipients present on the LNC-AG shell (50% compared to 30% for PNC-AG) may have produced a thicker wall which contributed to the slower release rates at the later stages of the experiment (Watnasirichaikul et al., 2002).

No drug leakage was observed from any of the NDDSs during the storage stability study (14 days at 4 °C) showing the robustness of the nanocarriers. Sizes of all the nanocarriers were also stable under the same conditions, and all of them remained monodispersed, demonstrating physical stability of the NDDSs. However, the AG concentration gradually decreased to 90% after 14 days at 4 °C in case of CL-AGs. Based on the difference in the formulation, EE and drug loading capacity of the liposomes, a large portion of the entrapped AG may be present at the surfaces of the CL-AG which puts the drug in contact of the aqueous environment during storage. This may lead to chemical modification or degradation, as pure apigenin is known to be an unstable molecule (Patel et al.,

2007) in aqueous environments with pH below 8.25 (Xu et al., 2006). Further study would be necessary to confirm the mechanism of the possible apigenin degradation. However, AG concentration did not alter throughout the experiment period for AL-AG, LNC-AG and PNC-AG. Therefore, these NDDSs can be used to improve aqueous solubility and stability of AG. None of the NDDSs showed any drug leakage at 4 °C up to 14 days.

The behavior of nanocarriers at the "bio-nano interface" must be evaluated to predict their i*n vivo* fate (Nel et al., 2009; Palchetti et al., 2016). Formation of protein corona around nanocarriers is dependent on their composition, diameter, shape and surface properties along with several experimental parameters, e.g protein concentration, temperature, incubation time and incubation condition (static vs dynamic) etc. (Caracciolo, 2015; Palchetti et al., 2016). From relatively small to huge amounts of proteins may get adsorbed on the nanovector surface, and if plasma opsonins are adsorbed, the NDDSs will be removed from the systemic circulation by the MPS (Palchetti et al., 2016). Additionally, NDDSs can be destabilized or form aggregates in presence of serum proteins which will alter their *in vivo* fate. After injection into systemic circulation, NDDSs will be dispersed, diluted and surrounded by high amounts of proteins very quickly. Therefore, it is necessary to keep nanocarrier concentration as low as possible, compared to serum proteins, while evaluating their stability in serum. The total concentration of serum proteins (average concentration calculated based on manufacture specifications) was 188 folds higher than concentration of the CL-AG, AL-AG and PNC-AG, and 75 folds higher than the LNC-AG, in the nanocarrier-FBS mixtures used in this study. None of the NDDSs showed any signs of particle aggregation or protein corona formation up to 6 h, which indicates that the PEG chains on their surface were adequate to efficiently repel the serum proteins. Although some peaks of larger aggregates were observed in DLS after 24 h in case of CL-AG, AL-AG and LNC-AG, it is not conclusive that they adsorbed proteins on their surface as the control FBS also showed peaks around 200–500 nm at this time point. The nanocarriers may gradually lose their ability to repel proteins due to desorption of PEG chains from their surface, which occurs in a time-dependent way (Nag and Awasthi, 2013; Nag et al., 2013). Conversely, the larger peaks on the NDDS-FBS mixture also may appear due to the aggregated particles from FBS, which overlapped the peaks of the nanocarriers and shifted the peaks toward a higher value. The PNC-AG did not show any signs of particle aggregation or protein adsorption up to 24 h, but its peak shifted slightly towards smaller diameter (approximately 35 nm). As the PNC-AG was prepared using nanoprecipitation technique, tiny aqueous cavities may get entrapped within its oily core (Rabanel et al., 2014). Water from NDDS core may not escape to the exterior during storage as the particle core and shell membrane are less fluid at colder storage temperature (therefore no change in particle size is observed during storage), but can gradually come out when the NDDS is at physiological temperature in presence of serum due to altered osmotic pressure (Wolfram et al., 2014). Finally, the experiment showed that all of the developed NDDSs (CL-AG, AL-AG, LNC-AG and PNC-AG) were stable after large dilution in serum and did not form significant aggregates or protein corona for extended period which demonstrates their prolonged stability in serum.

Additionally, complement consumption of the NDDSs in human serum was evaluated by CH50 assay, as high consumption can lead to a rapid activation of the complement system and can be followed by clearance from bloodstream. The CH50 assay is an efficient technique for measuring the activation of the total complement system. It correlates well with other complement activation evaluation methods i.e. crossed immunoelectrophoresis and enzyme-linked immunosorbent assay, and represents also a good preliminary experiment to predict the stealth properties of nanocarriers intended for systemic administration (Meerasa et al., 2011). However, previous studies reporting complement consumption of nanocarriers (Cajot et al., 2011; Vonarbourg et al., 2006) plotted percentage of CH50 unit consumption against theoretical surface area of the particles which was calculated using an arbitrary density value. In contrast, NTA was used in this study to determine the number of nanocarriers per mL of NHS. Surface area was calculated using this number and the mean diameter of the NDDS. The previous method of theoretical surface area calculation produced values much higher (1474–1616 cm^2/mL of NHS for the NDDS samples in this study) than the actual surface area obtained by NTA. Therefore, careful consideration is necessary when comparing the results with previous reports. The lowest CH50 unit consumption was observed for LNC-AG, which is in agreement with the results described by Vonarbourg et al. and can be possibly attributed to its smaller size (Vonarbourg et al., 2006) and higher percentage of PEG in its composition (due to presence of Kolliphor® HS15 and DSPE-$mPEG_{2000}$) (Jeon et al., 1991) compared to the other NDDSs. Although, mean diameter of CL-AG, AL-AG and PNC-AG were similar, their CH50 unit consumption was different. Complement consumption of CL-AG was comparable with AL-AG up to 600 cm^2/mL of NHS, but augmented comparatively faster then, possibly due to its positive surface-charge (Capriotti et al., 2012). Complement activation of PNC-AG was higher at surface area <600 cm^2 compared to other three NDDSs, but reached only 23.7% at 832 cm^2/mL of NHS. The difference can be due to several factors i.e. composition, PEG chain conformation, PEG density or presence of surfactant coating (PS80) (Gao and He, 2014). Further study would be necessary to validate the precise reason. Overall, the NDDSs did not show any strong complement consumption and should not be rapidly removed from systemic circulation by MPS.

Toxicity of the NDDSs on a human endothelial cell line (EAhy926) was evaluated to assess their injectability. The commonly used cytotoxic assays works by different mechanisms and their sensitivity can be dissimilar with alteration of cell lines (Fotakis and Timbrell, 2006; Lappalainen et al., 1994; Lobner, 2000). Moreover, presence of nanoparticles (Holder et al., 2012; Kroll et al., 2009) or the drug molecule (Wang et al., 2010) may interfere with the assay procedures and provide misleading results. Therefore, two common cytotoxicity assays i.e. MTS and LDH assays were used for evaluation and comparison of the possible toxic effects of the NDDSs on the endothelial cells. The two methods for cytotoxicity assessment provided similar results. Among the NDDSs, only CL-AG showed significant toxicity in a dose dependent manner in both assays at concentrations above 171 μg/mL. This is probably due to the presence of the tertiary nitrogen group containing cationic cholesterol derivative (DC-Chol) in CL-AG, which can act as protein kinase C inhibitor and result toxicity (Lv et al., 2006). In comparison, the AL-AG, LNC-AG and PNC-AG were nontoxic at their maximum test concentrations (420, 436 and 189 μg/mL respectively). Overall, the NDDSs were nontoxic up to high concentrations and can be considered suitable as injectable AG-loaded nanovectors.

5. Conclusion

In this study, novel AG-loaded NDDSs, i.e. liposomes, LNC and PNC were developed as potential injectable dosage forms of AG. The nanovectors were characterized by their size, surface charge, EE, mass yield and drug loading capacity. Moreover, drug release property, drug leakage possibility and stability during storage were evaluated. Furthermore, stability of the NDDSs in serum at physiological temperature and cytotoxicity on a human macro-vascular endothelial cell line was evaluated. The size of all the NDDSs was within the acceptable limit for injectable nanocarriers.

The surface of the nanocarriers was positively (CL-AG) or negatively charged (AL-AG, LNC-AG and PNC-AG) which hinder particle aggregation and provided stability during storage. Presence of DC-Chol showed significant increase in AG entrapment at physiological pH, and application of such cationic lipids to improve AG encapsulation can be utilized in future NDDS development of the drug. Although, toxicity due to cationic lipids and chemical stability of the drug have to be carefully considered. Presence of oily core in the NDDSs was beneficial for AG encapsulation, and the LNC-AG and PNC-AG showed high EE. Moreover, this is the first study reporting the suitability and use of the tocopherol grafted PEG-b-polyphosphate amphiphilic block-copolymer PEG_{120}-b-$(PBP\text{-}co\text{-}Ptoco)_9$ for stable nanocapsule preparation.

Finally, all the nanovectors were stable in FBS for extended periods, showed weak complement system activation and were non-toxic to human macrovascular endothelial cells up to high concentrations, and therefore were suitable as injectable nanocarriers of AG. Due to less pronounced burst effect and extended release characteristics, the nanocapsule formulations i.e. LNC-AG and PNC-AG could be favorable approach for achieving prolonged pharmacological activity or tumor-targeted delivery of AG using injectable NDDS.

Funding

This work was supported by the NanoFar Consortium of the Erasmus Mundus program; and Fonds Léon Fredericq, CHU, University of Liege, Liege, Belgium. CERM is indebted to the Interreg Euregio Meuse-Rhine IV-A consortium BioMIMedics (2011–2014) and IAP VII-05 (FS2) for supporting research on new degradable polymers.

Appendix A. Supplementary data

Supplementary data associated with this article can be found, in the online version, at http://dx.doi.org/10.1016/j.ijpharm.2017.04.064

References

Allard, E., Passirani, C., Garcion, E., Pigeon, P., Vessieres, A., Jaouen, G., Benoit, J.P., 2008. Lipid nanocapsules loaded with an organometallic tamoxifen derivative as a novel drug-carrier system for experimental malignant gliomas. J. Control. Release 130, 146–153.

Baeten, E., Vanslambrouck, S., Jérôme, C., Lecomte, P., Junkers, T., 2016. Anionic flow polymerizations toward functional polyphosphoesters in microreactors: polymerization and UV-modification. Eur. Polym. J. 80, 208–218.

Bellavance, M.A., Poirier, M.B., Fortin, D., 2010. Uptake and intracellular release kinetics of liposome formulations in glioma cells. Int. J. Pharm. 395, 251–259.

Cajot, S., Lautram, N., Passirani, C., Jerome, C., 2011. Design of reversibly core cross-linked micelles sensitive to reductive environment. J. Control. Release 152, 30–36.

Capriotti, A.L., Caracciolo, G., Cavaliere, C., Foglia, P., Pozzi, D., Samperi, R., Lagana, A., 2012. Do plasma proteins distinguish between liposomes of varying charge density. J. Proteomics 75, 1924–1932.

Caracciolo, G., 2015. Liposome-protein corona in a physiological environment: challenges and opportunities for targeted delivery of nanomedicines. Nanomedicine 11, 543–557.

Clement, B., Grignard, B., Koole, L., Jérôme, C., Lecomte, P., 2012. Metal-free strategies for the synthesis of functional and well-defined polyphosphoesters. Macromolecules 45, 4476–4486.

De Melo, N.F., De Araujo, D.R., Grillo, R., Moraes, C.M., De Matos, A.P., de Paula, E., Rosa, A.H., Fraceto, L.F., 2012. Benzocaine-loaded polymeric nanocapsules: study of the anesthetic activities. J. Pharm. Sci. 101, 1157–1165.

Eavarone, D.A., Yu, X., Bellamkonda, R.V., 2000. Targeted drug delivery to C6 glioma by transferrin-coupled liposomes. J. Biomed. Mater. Res. 51, 10–14.

Engelmann, C., Blot, E., Panis, Y., Bauer, S., Trochon, V., Nagy, H., Lu, H., Soria, C., 2002. Apigenin-strong cytostatic and anti-angiogenic action in vitro contrasted by lack of efficacy *in vivo*. Phytomedicine 9, 489–495.

Favaro, G., Clementi, C., Romani, A., Vickackaite, V., 2007. Acidichromism and ionochromism of luteolin and apigenin, the main components of the naturally occurring yellow weld: a spectrophotometric and fluorimetric study. J. Fluoresc. 17, 707–714.

Felgner, P.L., Ringold, G.M., 1989. Cationic liposome-mediated transfection. Nature 337, 387–388.

Fotakis, G., Timbrell, J.A., 2006. *In vitro* cytotoxicity assays: comparison of LDH, neutral red, MTT and protein assay in hepatoma cell lines following exposure to cadmium chloride. Toxicol. Lett. 160, 171–177.

Fu, J.Y., Blatchford, D.R., Tetley, L., Dufes, C., 2009. Tumor regression after systemic administration of tocotrienol entrapped in tumor-targeted vesicles. J. Control. Release 140, 95–99.

Gao, H., He, Q., 2014. The interaction of nanoparticles with plasma proteins and the consequent influence on nanoparticles behavior. Expert Opin. Drug Deliv. 11, 409–420.

Gradolatto, A., Canivenc-Lavier, M.C., Basly, J.P., Siess, M.H., Teyssier, C., 2004. Metabolism of apigenin by rat liver phase I and phase ii enzymes and by isolated perfused rat liver. Drug Metab. Dispos. 32, 58–65.

Gradolatto, A., Basly, J.P., Berges, R., Teyssier, C., Chagnon, M.C., Siess, M.H., Canivenc-Lavier, M.C., 2005. Pharmacokinetics and metabolism of apigenin in female and male rats after a single oral administration. Drug Metab. Dispos. 33, 49–54.

He, C., Hu, Y., Yin, L., Tang, C., Yin, C., 2010. Effects of particle size and surface charge on cellular uptake and biodistribution of polymeric nanoparticles. Biomaterials 31, 3657–3666.

Heurtault, B., Saulnier, P., Pech, B., Venier-Julienne, M.-C., Proust, J.-E., Phan-Tan-Luu, R., Benoît, J.-P., 2003. The influence of lipid nanocapsule composition on their size distribution. Eur. J. Pharm. Sci. 18, 55–61.

Holder, A.L., Goth-Goldstein, R., Lucas, D., Koshland, C.P., 2012. Particle-induced artifacts in the MTT and LDH viability assays. Chem. Res. Toxicol. 25, 1885–1892.

Iyer, A.K., Khaled, G., Fang, J., Maeda, H., 2006. Exploiting the enhanced permeability and retention effect for tumor targeting. Drug Discov. Today 11, 812–818.

Jeon, S.I., Lee, J.H., Andrade, J.D., De Gennes, P.G., 1991. Protein–surface interactions in the presence of polyethylene oxide. J. Colloid Interface Sci. 142, 149–158.

Karim, R., Palazzo, C., Evrard, B., Piel, G., 2016. Nanocarriers for the treatment of glioblastoma multiforme: current state-of-the-art. J. Control. Release 227, 23–37.

Karim, R., Somani, S., Al Robaian, M., Mullin, M., Amor, R., McConnell, G., Dufes, C., 2017. Tumor regression after intravenous administration of targeted vesicles entrapping the vitamin E α-tocotrienol. J. Control. Release 246, 79–87.

Kroll, A., Pillukat, M.H., Hahn, D., Schnekenburger, J., 2009. Current in vitro methods in nanoparticle risk assessment: limitations and challenges. Eur. J. Pharm. Biopharm. 72, 370–377.

Lainé, A.-L., Clavreul, A., Rousseau, A., Tétaud, C., Vessieres, A., Garcion, E., Jaouen, G., Aubert, L., Guilbert, M., Benoit, J.-P., 2014. Inhibition of ectopic glioma tumor growth by a potent ferrocenyl drug loaded into stealth lipid nanocapsules. Nanomedicine 10, 1667–1677.

Laine, A.L., Gravier, J., Henry, M., Sancey, L., Bejaud, J., Pancani, E., Wiber, M., Texier, I., Coll, J.L., Benoit, J.P., Passirani, C., 2014. Conventional versus stealth lipid nanoparticles: formulation and in vivo fate prediction through FRET monitoring. J. Control. Release 188, 1–8.

Lamprecht, A., Bouligand, Y., Benoit, J.P., 2002. New lipid nanocapsules exhibit sustained release properties for amiodarone. J. Control. Release 84, 59–68.

Lappalainen, K., Jaaskelainen, I., Syrjanen, K., Urtti, A., Syrjanen, S., 1994. Comparison of cell proliferation and toxicity assays using two cationic liposomes. Pharm. Res. 11, 1127–1131.

Lee, J.H., Zhou, H.Y., Cho, S.Y., Kim, Y.S., Lee, Y.S., Jeong, C.S., 2007. Anti-inflammatory mechanisms of apigenin: inhibition of cyclooxygenase-2 expression, adhesion of monocytes to human umbilical vein endothelial cells, and expression of cellular adhesion molecules. Arch. Pharm. Res. 30, 1318–1327.

Lertsutthiwong, P., Noomun, K., Jongaroonngamsang, N., Rojsitthisak, P., Nimmannit, U., 2008. Preparation of alginate nanocapsules containing turmeric oil. Carbohydr. Polym. 74, 209–214.

Li, B., Robinson, D.H., Birt, D.F., 1997. Evaluation of properties of apigenin and [G-3H] apigenin and analytic method development. J. Pharm. Sci. 86, 721–725.

Li, F., Zhao, X., Wang, H., Zhao, R., Ji, T., Ren, H., Anderson, G.J., Nie, G., Hao, J., 2015. Multiple layer-by-layer lipid-polymer hybrid nanoparticles for improved FOLFIRINOX chemotherapy in pancreatic tumor models. Adv. Funct. Mater. 25, 788–798.

Lim, L.Y., Koh, P.Y., Somani, S., Al Robaian, M., Karim, R., Yean, Y.L., Mitchell, J., Tate, R. J., Edrada-Ebel, R., Blatchford, D.R., Mullin, M., Dufes, C., 2015. Tumor regression following intravenous administration of lactoferrin- and lactoferricin-bearing dendriplexes. Nanomedicine 11, 1445–1454.

Lobner, D., 2000. Comparison of the LDH and MTT assays for quantifying cell death: validity for neuronal apoptosis? J. Neurosci. Methods 96, 147–152.

Lopalco, A., Ali, H., Denora, N., Rytting, E., 2015. Oxcarbazepine-loaded polymeric nanoparticles: development and permeability studies across in vitro models of the blood-brain barrier and human placental trophoblast. Int. J. Nanomed. 10, 1985–1996.

Lv, H., Zhang, S., Wang, B., Cui, S., Yan, J., 2006. Toxicity of cationic lipids and cationic polymers in gene delivery. J. Control. Release 114, 100–109.

Meerasa, A.G., Huang, J.X., Gu, F., 2011. CH50: A revisited hemolytic complement consumption assay for evaluation of nanoparticles and blood plasma protein interaction. Curr. Drug Deliv. 8, 290–298.

Moore, T.L., Rodriguez-Lorenzo, L., Hirsch, V., Balog, S., Urban, D., Jud, C., Rothen-Rutishauser, B., Lattuada, M., Petri-Fink, A., 2015. Nanoparticle colloidal stability in cell culture media and impact on cellular interactions. Chem. Soc. Rev. 44, 6287–6305.

Mora-Huertas, C.E., Fessi, H., Elaissari, A., 2010. Polymer-based nanocapsules for drug delivery. Int. J. Pharm. 385, 113–142.

Mora-Huertas, C.E., Garrigues, O., Fessi, H., Elaissari, A., 2012. Nanocapsules prepared via nanoprecipitation and emulsification-diffusion methods: comparative study. Eur. J. Pharm. Biopharm. 80, 235–239.
Mosqueira, V.C., Legrand, P., Morgat, J.L., Vert, M., Mysiakine, E., Gref, R., Devissaguet, J.P., Barratt, G., 2001. Biodistribution of long-circulating PEG-grafted nanocapsules in mice: effects of PEG chain length and density. Pharm. Res. 18, 1411–1419.
Nag, O.K., Awasthi, V., 2013. Surface engineering of liposomes for stealth behavior. Pharmaceutics 5, 542–569.
Nag, O.K., Yadav, V.R., Hedrick, A., Awasthi, V., 2013. Post-modification of preformed liposomes with novel non-phospholipid poly(ethylene glycol)-conjugated hexadecylcarbamoylmethyl hexadecanoic acid for enhanced circulation persistence in vivo. Int. J. Pharm. 446, 119–129.
Nel, A.E., Madler, L., Velegol, D., Xia, T., Hoek, E.M., Somasundaran, P., Klaessig, F., Castranova, V., Thompson, M., 2009. Understanding biophysicochemical interactions at the nano-bio interface. Nat. Mater. 8, 543–557.
Palchetti, S., Colapicchioni, V., Digiacomo, L., Caracciolo, G., Pozzi, D., Capriotti, A.L., La Barbera, G., Lagana, A., 2016. The protein corona of circulating PEGylated liposomes. Biochim. Biophys. Acta 1858, 189–196.
Papay, Z.E., Sebestyen, Z., Ludanyi, K., Kallai, N., Balogh, E., Kosa, A., Somavarapu, S., Boddi, B., Antal, I., 2016. Comparative evaluation of the effect of cyclodextrins and pH on aqueous solubility of apigenin. J. Pharm. Biomed. Anal. 117, 210–216.
Patel, D., Shukla, S., Gupta, S., 2007. Apigenin and cancer chemoprevention: progress, potential and promise (review). Int. J. Oncol. 30, 233–245.
Peer, D., Karp, J.M., Hong, S., Farokhzad, O.C., Margalit, R., Langer, R., 2007. Nanocarriers as an emerging platform for cancer therapy. Nat. Nanotechnol. 2, 751–760.
Rabanel, J.M., Hildgen, P., Banquy, X., 2014. Assessment of PEG on polymeric particles surface, a key step in drug carrier translation. J. Control. Release 185, 71–87.
Romanova, D., Vachalkova, A., Cipak, L., Ovesna, Z., Rauko, P., 2001. Study of antioxidant effect of apigenin, luteolin and quercetin by DNA protective method. Neoplasma 48, 104–107.
Senior, J., Crawley, J.C., Gregoriadis, G., 1985. Tissue distribution of liposomes exhibiting long half-lives in the circulation after intravenous injection. Biochim. Biophys. Acta 839, 1–8.
Sharma, A., Sharma, U.S., Straubinger, R.M., 1996. Paclitaxel-liposomes for intracavitary therapy of intraperitoneal P388 leukemia. Cancer Lett. 107, 265–272.
Shukla, S., Gupta, S., 2010. Apigenin: a promising molecule for cancer prevention. Pharm. Res. 27, 962–978.
Straubinger, R.M., Sharma, A., Murray, M., Mayhew, E., 1993. Novel taxol formulations: taxol-containing liposomes. J. Natl. Cancer Inst. 69–78.
Tripodo, G., Pasut, G., Trapani, A., Mero, A., Lasorsa, F.M., Chlapanidas, T., Trapani, G., Mandracchia, D., 2015. Inulin-D-alpha-tocopherol succinate (INVITE) nanomicelles as a platform for effective intravenous administration of curcumin. Biomacromolecules 16, 550–557.
Tungjai, M., Poompimon, W., Loetchutinat, C., Kothan, S., Dechsupa, N., Mankhetkorn, S., 2008. Spectrophotometric characterization of behavior and the predominant species of flavonoids in physiological buffer: determination of solubility, lipophilicity and anticancer efficacy. Open Drug Deliv. J. 2, 10–19.
Vanslambrouck, S., 2015. Polyphosphate-based Amphiphilic Copolymers: Synthesis and Application to Drug Nanocarriers. University of Liège, Liège, Belgium.
Vonarbourg, A., Passirani, C., Saulnier, P., Simard, P., Leroux, J.C., Benoit, J.P., 2006. Evaluation of pegylated lipid nanocapsules versus complement system activation and macrophage uptake. J. Biomed. Mater. Res. 78, 620–628.
Wan, L., Guo, C., Yu, Q., Li, Y., Wang, X., Wang, X., Chen, C., 2007. Quantitative determination of apigenin and its metabolism in rat plasma after intravenous bolus administration by HPLC coupled with tandem mass spectrometry. J. Chromatogr. B 855, 286–289.
Wang, P., Henning, S.M., Heber, D., 2010. Limitations of MTT and MTS-based assays for measurement of antiproliferative activity of green tea polyphenols. PLoS One 5, e10202.
Watnasirichaikul, S., Rades, T., Tucker, I.G., Davies, N.M., 2002. Effects of formulation variables on characteristics of poly (ethylcyanoacrylate) nanocapsules prepared from w/o microemulsions. Int. J. Pharm. 235, 237–246.
Wei, X., Gao, J., Zhan, C., Xie, C., Chai, Z., Ran, D., Ying, M., Zheng, P., Lu, W., 2015. Liposome-based glioma targeted drug delivery enabled by stable peptide ligands. J. Control. Release 218, 13–21.
Wolfram, J., Suri, K., Yang, Y., Shen, J., Celia, C., Fresta, M., Zhao, Y., Shen, H., Ferrari, M., 2014. Shrinkage of pegylated and non-pegylated liposomes in serum. Colloids Surf. B Biointerfaces 114, 294–300.
Xu, X., Yu, L., Chen, G., 2006. Determination of flavonoids in Portulaca oleracea L by capillary electrophoresis with electrochemical detection. J. Pharm. Biomed. Anal. 41, 493–499.
Yilmaz, Z.E., Jerome, C., 2016. Polyphosphoesters: new trends in synthesis and drug delivery applications. Macromol. Biosci. 16, 1745–1761.
Yilmaz, Z.E., Vanslambrouck, S., Cajot, S., Thiry, J., Debuigne, A., Lecomte, P., Jérôme, C., Riva, R., 2016. Core cross-linked micelles of polyphosphoester containing amphiphilic block copolymers as drug nanocarriers. RSC Adv. 6, 42081–42088.
Yuan, J.-L., Liu, Z.-G., Hu, Z., Zou, G.-L., 2007. Study on interaction between apigenin and human serum albumin by spectroscopy and molecular modeling. J. Photochem. Photobiol. A: Chem. 191, 104–113.
Zanotto-Filho, A., Coradini, K., Braganhol, E., Schroder, R., de Oliveira, C.M., Simoes-Pires, A., Battastini, A.M., Pohlmann, A.R., Guterres, S.S., Forcelini, C.M., Beck, R. C., Moreira, J.C., 2013. Curcumin-loaded lipid-core nanocapsules as a strategy to improve pharmacological efficacy of curcumin in glioma treatment. Eur. J. Pharm. Biopharm. 83, 156–167.
Zhang, L., Gu, F.X., Chan, J.M., Wang, A.Z., Langer, R.S., Farokhzad, O.C., 2008. Nanoparticles in medicine: therapeutic applications and developments. Clin. Pharmacol. Ther. 83, 761–769.
Zhang, J., Liu, D., Huang, Y., Gao, Y., Qian, S., 2012. Biopharmaceutics classification and intestinal absorption study of apigenin. Int. J. Pharm. 436, 311–317.
Zhang, J., Huang, Y., Liu, D., Gao, Y., Qian, S., 2013. Preparation of apigenin nanocrystals using supercritical antisolvent process for dissolution and bioavailability enhancement. Eur. J. Pharm. Sci. 48, 740–747.
Zhao, L., Zhang, L., Meng, L., Wang, J., Zhai, G., 2013. Design and evaluation of a self-microemulsifying drug delivery system for apigenin. Drug Dev. Ind. Pharm. 39, 662–669.
Zheng, P.-W., Chiang, L.-C., Lin, C.-C., 2005. Apigenin induced apoptosis through p53-dependent pathway in human cervical carcinoma cells. Life Sci. 76, 1367–1379.